Toward a Time-Dependent Probabilistic Seismic Hazard Analysis for Alaska

Oliver S. Boyd, Yuehua Zeng, Charles G. Bufe, and Robert L. Wesson

U.S. Geological Survey, Golden, Colorado, USA

Fred Pollitz and Jeanne L. Hardebeck

U.S. Geological Survey, Menlo Park, California, USA

We report on a time-dependent seismic hazard analysis for Alaska and the Aleutians to complement our recently completed time-independent map. Whereas the time-independent map treats all sources as statistically independent, the time-dependent analysis is based on calculations of the conditional probability of occurrence for the next 50 years by using a Brownian Passage Time model for the seismic sources judged to be characteristic. We then consider how those probabilities are modified by coseismic and postseismic stress changes resulting from large regional earthquakes occurring from 1938 to 2002. Recombining the time-dependent probabilities with time-independent truncated Gutenberg–Richter and smoothed seismicity sources leads to our time-dependent probabilistic seismic hazard results. We find that when accounting for time dependence without stress changes, earthquake probabilities can be significantly altered, reducing probabilities to near zero or increasing them to several times the time-independent values. In addition, accounting for coseismic stress changes tends to have a local influence on earthquake probabilities, whereas postseismic effects can be far-reaching in both time and space. In sum, however, since we combine time-dependent and time-independent sources, the modification to seismic hazard is relatively minor, increasing or decreasing hazard adjacent to characteristic faults by about 10%. Most cities, located far from characteristic faults, are little affected.

1. INTRODUCTION

Time-independent probabilistic seismic hazard maps for Alaska were prepared in 1985 [*Thenhaus et al.*, 1985] and 1999 [*Wesson et al.*, 1999], and recently revised in 2007 [*Wesson et al.*, 2007], taking into account new recurrence information [*Matmon et al.*, 2006] and ground motion relationships [*Frankel et al.*, 2002]. The recent M_w 7.9 2002 Denali fault earthquake [*Eberhart-Phillips et al.*, 2003; *Haeussler et al.*, 2004a], having a recurrence interval on the order of 650 years, has revived an effort to account for the time dependence of earthquake probabilities in a probabilistic seismic hazard assessment (PSHA) of Alaska. In this study, we have prepared a time-dependent probabilistic seismic hazard analysis, which accounts for characteristic fault behavior and viscoelastic stress perturbations resulting from nine regional earthquakes occurring from 1938 to 2002.

Active Tectonics and Seismic Potential of Alaska
Geophysical Monograph Series 179

10.1029/179GM23

The state of Alaska rests at the northern end of the convergent margin between the North American and Pacific plates. At a subduction rate of roughly 50 mm/yr [*DeMets and Dixon*, 1999], Alaska includes the most abundant seismicity and highest rates of deformation in North America. Subduction gives way to right-lateral strike-slip deformation to the southeast along the Fairweather and Queen Charlotte faults. These faults extend into the interior of Alaska, the deformation being eventually transferred to the Totschunda and Denali faults with slip rates of about 10 mm/yr [*Matmon et al.*, 2006] (Plate 1).

Among Alaska's abundant seismicity are 16 earthquakes greater than magnitude 7.4 occurring since 1938. The nine earthquakes used for this study are shown in Plate 2. Excluding a small but significant region between the Fairweather fault and Prince William Sound, these 16 earthquakes have ruptured the entire plate margin extending from the western Aleutians to the Queen Charlotte Islands in southeast Alaska. The largest, having a magnitude of 9.2, occurred in 1964, where a large portion of the Alaskan subduction zone interface near Prince William Sound ruptured with displacements on the fault approaching 20 m [*Johnson et al.*, 1996]. The next largest earthquakes include the 1965 M 8.7 Rat Islands earthquake that ruptured the western Aleutians and the 1957 M 8.6 earthquake that ruptured the central Aleutians. These earthquakes, however, are located far from population centers, and there is some debate as to the regular repeatability of large earthquakes in the central and western Aleutians [*Wesson et al.*, 2007] as is evidenced by subsequent large overlapping ruptures. To the southeast along the Fairweather–Queen Charlotte fault system, large earthquakes occur frequently as a result of slip rates of almost 50 mm/yr [*DeMets and Dixon*, 1999], the most recent of which occurred in 1972. One of the most recent and notable earthquakes was located on the Denali fault midway between Anchorage and Fairbanks. The M_w 7.9 earthquake occurred on November 3, 2002, had 340 km of surface rupture, and had local slip exceeding 8 m [*Haeussler et al.*, 2004b]. Postseismic deformation subsequent to the Denali earthquake has been observed and modeled to infer the subsurface rheology [*Freed et al.*, 2006; *Pollitz*, 2005], the results of which are used in the present study.

2. OVERVIEW OF METHODOLOGY

2.1. Characteristic Earthquake Behavior

Schwartz and Coppersmith [1984] suggested that earthquakes on fault segments tend to occur in a characteristic manner, that is, earthquakes on a particular fault segment rupture over a narrow range of magnitude with a narrow range of recurrence interval. This is in stark contrast to Gutenberg–Richter recurrence behavior, which is seen in background seismicity, where earthquakes occur with an exponential distribution of magnitudes (e.g., magnitude 5 being 10 times more likely than a magnitude 6 assuming a slope or b value of 1). Characteristic behavior, if substantiated, lends itself to developing a time-dependent PSHA, such as that presented by *Cramer et al.* [2000]. Taking into account the characteristic and time-dependent behavior of faults, they estimate that the probability of exceeding a given amount of ground motion in California over a given period can increase or decrease by a factor of 2. As will be shown in a subsequent section, depending on the parameters that describe recurrence, the effects of characteristic earthquake behavior can result in much greater changes to earthquake probability.

2.2. Effects of Stress Transfer

In addition to periodic earthquake recurrence on characteristic fault segments, stress changes on these fault segments due to regional earthquakes can alter time-dependent probabilistic seismic hazard estimates. *Toda et al.* [1998], for example, estimated the effect of the Kobe earthquake on earthquake probability for major faults in Japan. *Parsons et al.* [2000], in addition to accounting for the mean and standard deviation of the characteristic return period of earthquakes on faults near Istanbul, Turkey, modeled the stress transfer due to faulting on neighboring fault segments. This work was motivated by the observation that there was a westward progression of faulting in the region, presumably due to a transfer of stress from one fault segment to its neighbor to the west [*Stein et al.*, 1997]. Observations that seismicity subsequent to a major event was concentrated in calculated regions of positive Coulomb stress change [*Harris and Simpson*, 1992; *King et al.*, 1994; *Reasenberg and Simpson*, 1992], defined as the shear stress change promoting failure minus the normal stress change, moderated by the effective coefficient of friction, inhibiting failure, support the notion of stress transfer. *Parsons et al.* [2000] estimated the current state of stress in the region and used this to calculate the probability of strong shaking (modified Mercalli intensity >VIII) in Istanbul. In contrast to a time-independent analysis suggesting that the probability of strong shaking in the next 30 years is 20 ± 5%, the time-dependent analysis assuming characteristic sources but no stress transfer increases the probability to 49 ± 15%. Accounting for coseismic stress transfer, the probability is elevated to 62 ± 15%. The importance of stress transfer depends strongly on the location, orientation, and sense of slip on target faults. For example, the Kobe, Japan, earthquake

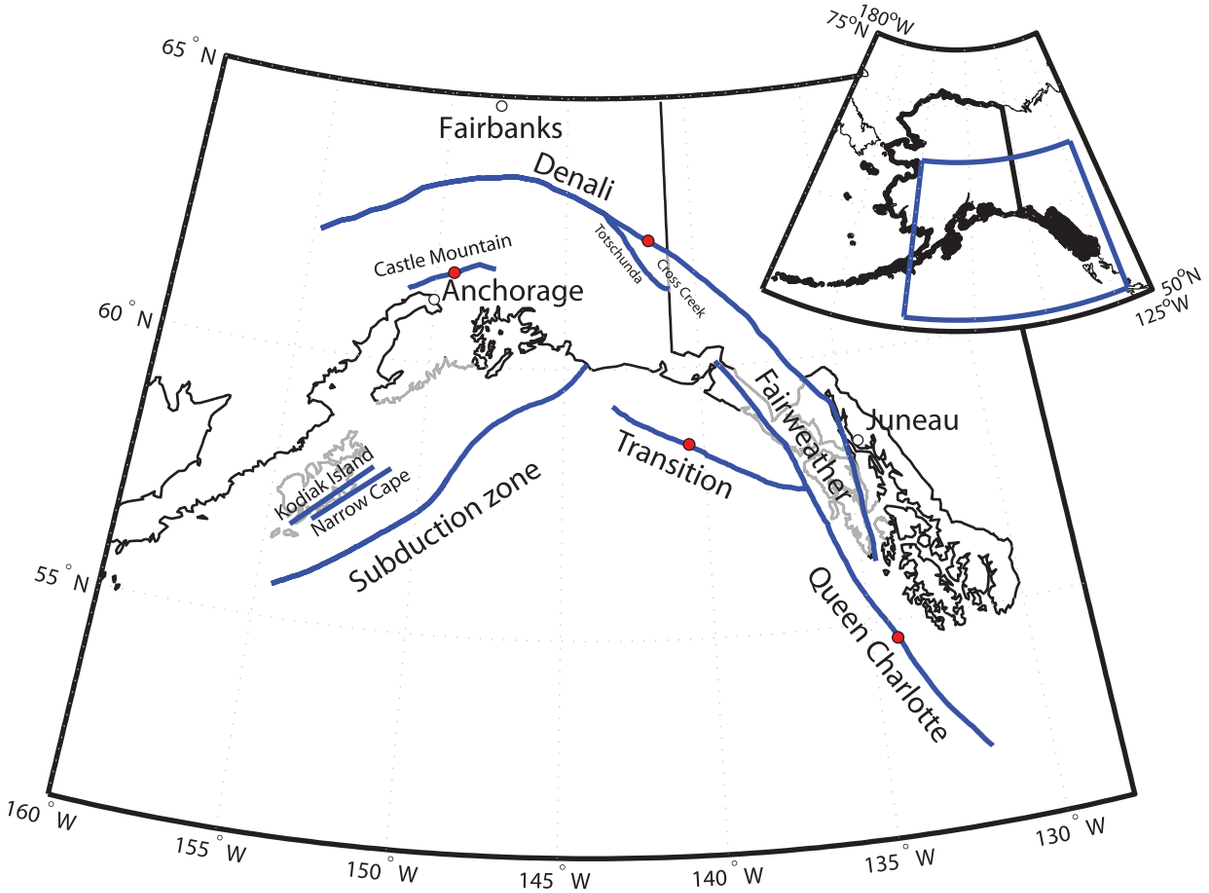

Plate 1. Map of Alaska with target faults in blue. The red circles are the locations for the analyses in Plates 3–5. The inset in the upper right corner shows the state of Alaska (thick black line) and the study area (blue box).

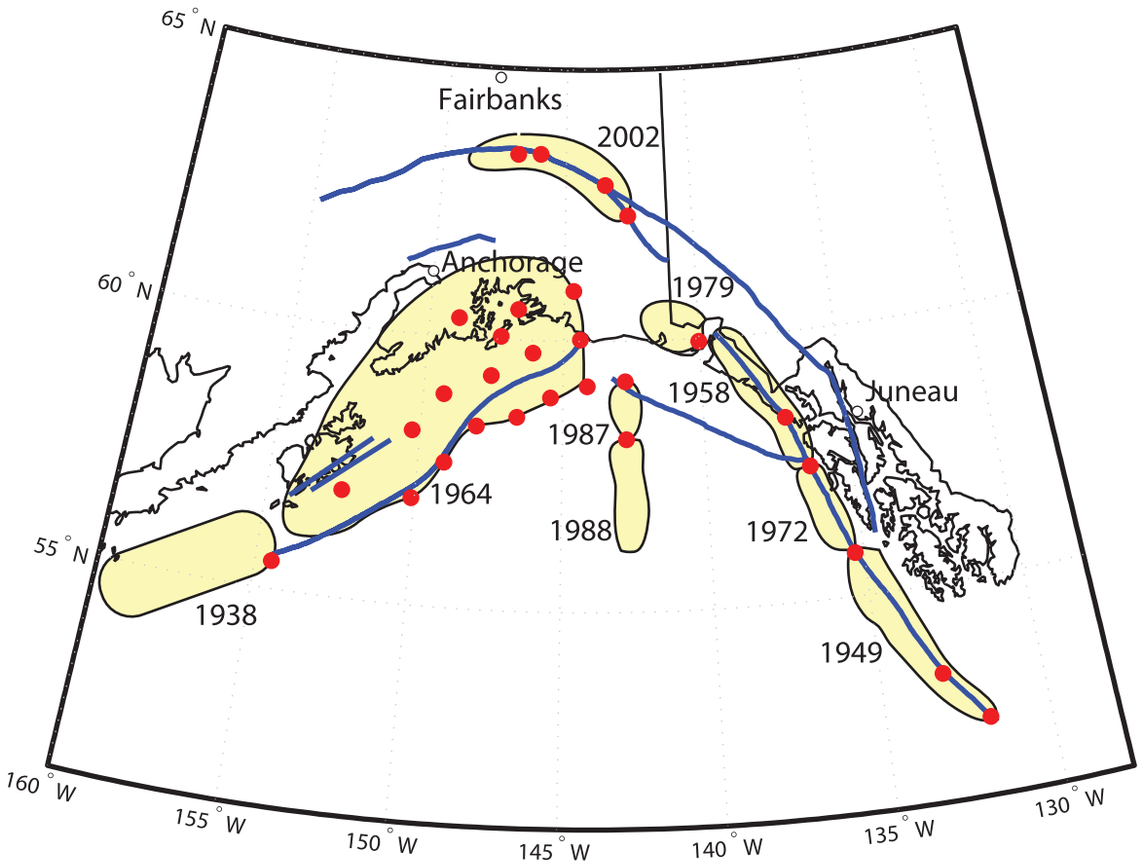

Plate 2. Map of Alaska with earthquake sources. Red dots are source segment corners with the geometry specified in Table 2. The approximate area of the combined source is outlined in yellow. Blue lines are target faults.

decreased the probability of earthquakes on some faults, while increasing it on others [*Toda et al.*, 1998].

An earthquake rupture does not only redistribute stress near the Earth's surface through elastic rebound, as was implemented by *Parsons et al.* [2000], but also, through inelastic processes, redistributes stress over time to great depths through the crust and into the upper mantle. *Harris and Simpson* [1996], *Jaume and Sykes* [1996], and *Stein* [1999] suggest that coseismic elastic stress changes can have a lasting effect on probability (e.g., via stress shadows). Other studies [e.g., *Freed and Lin*, 2001; *Pollitz and Sacks*, 1997, 2002] suggest that viscoelastic stress transfer may play an important role over the long term. The loading and relaxation of the ductile portion of the mantle lithosphere further modifies the stress field leading to a perturbation of the seismic hazard [e.g., *Michael*, 2005]. *Pollitz et al.* [2001], for example, observed surface deformation with GPS and InSAR (interferometric synthetic aperture radar) for up to 3 years after the magnitude 7.1 1999 Hector Mine earthquake. They found significant deformation on the order of 40 mm/yr up to 100 km away from the epicenter. *Kenner* [2004] performed a similar analysis for the effect of lower crustal and upper mantle relaxation on fault loading after the 1906 San Francisco earthquake. She concludes that relaxation of the lower crust and upper mantle after a characteristic earthquake can contribute between 60% and 80% of the stress released in a subsequent recurrence. Recent calculations incorporating rate- and state-dependent friction and Brownian Passage Time (BPT) renewal [*Hardebeck*, 2004; *Parsons*, 2005] suggest that coseismic stress changes alone may not have a long-term effect on earthquake probability and that continuing postseismic relaxation should be included in earthquake triggering models.

3. COMPONENTS OF THE ANALYSIS

Our method of producing a time-dependent hazard map is to incorporate time dependence into those elements that we think are time-dependent or have enough information to be treated as time-dependent. The remainder of the analysis is time-independent. For a complete discussion on the issues involved in making a time-independent hazard map for Alaska, please see *Wesson et al.* [this issue].

3.1. Sources

Faults for which geometry and slip rate are known are explicitly included. Other sources, presumably faults but with unknown geometry or slip rate, are characterized by the location and rate of background seismicity. The latter of these sources is referred to as "smoothed seismicity" since earthquakes are spread over a region, typically with a 50-km smoothing kernel or uniformly in an areal source zone. Recurrence of a given magnitude is defined with a Gutenberg–Richter relationship, $\log_{10}(n) = am + b$, where the $\log_{10}$ of the number of earthquakes, n, in a given magnitude interval, m, is equal to the a value times the magnitude plus the b value. For a full description of the seismic sources used in this study, see *Wesson et al.* [2007].

3.1.1. Smoothed seismicity. We use an updated declustered catalog [*Gardner and Knopoff*, 1974], which combines events derived from instrumental seismicity since 1964. Sources of this catalog are *Engdahl and Villaseñor's* [2002] International Association for Seismology and Physics of the Earth's Interior (IASPEI) project, *Stover and Coffman*'s [1993] Seismicity of the United States, the U.S. Geological Survey Preliminary Determination of Epicenters (PDE), the International Seismological Centre (ISC), and the Alaska Earthquake Information Center (AEIC). The catalog is then split into three depth intervals: 0–50, 50–80, and 80–120 km. Those in the shallowest depth interval that lie along the subduction zone were sequestered for use with a different set of ground-motion relationships and a smoothed b value. Smoothed a values were then determined for each depth interval for use in a truncated Gutenberg–Righter recurrence relation. We consider the background seismicity to be time-independent although it may be argued that it is in fact time-dependent, since it only considers instrumental seismicity recorded from 1964 to 2004.

3.1.2. Fault sources. Faults for which slip rates can be estimated and recurrence information inferred include the Queen Charlotte, Fairweather, Totschunda, Denali, Castle Mountain, Kodiak Island, and Narrow Cape strike-slip faults, and the Transition Zone and Aleutian subduction zone thrust faults (Plate 1). All of these faults are given equal weight of Gutenberg–Richter and characteristic recurrence behavior with the exception of the Transition fault and the 1964 and Kodiak segments of the Aleutian subduction zone, which only have a characteristic component above magnitude 8. The characteristic part of the calculation has been modified to account for time-dependent earthquake probabilities and so acts as a moderate perturbation to the time-independent analysis. The equal weighting of characteristic and Gutenberg–Richter behavior is used to minimize the influence of time dependence since critical parameters are not well established. Parameters relevant to these fault sources are shown in Table 1.

3.1.3. Accounting for variable source parameters. Observations of the 2002 Denali earthquake and subsequent studies motivated modifications to the standard approach to

Table 1. Fault Segments Considered for Time-Dependent Analysis

Fault Name	Characteristic magnitude, M_o	Slip Rate, mm/yr	Recurrence Interval, yr	Year of Last Earthquake	Average Dip, deg
Queen Charlotte	8.0	49.0	149	1949	90
Fairweather offshore	8.0	49.5	147	1972	90
Fairweather onshore	8.0	48.0	152	1958	90
N Eastern Denali	7.9	8.4	650[a]	1682	90
S Eastern Denali	7.9	2.0	2730	642	90
Western Denali[b]	7.9	0.6	325[a]	1845	90
W Central Denali[b]	7.9	5.5	325[a]	2002	90
E Central Denali[b]	7.9	8.4	325[a]	2002	90
Western Denali[c]	7.9	0.4	325[a]	1845	90
W Central Denali[c]	7.9	3.9	325[a]	2002	90
E Central Denali[c]	7.9	6.0	325[a]	2002	90
Totschunda	7.9	6.0	650[a]	2002	90
Cross Creek	7.9	6.0	650	1682	90
E Castle Mountain	7.1	0.5	3770	122	75
Castle Mountain	7.1	2.9	650	1682	75
Transition fault	8.2	6.0	325	1845	10
1964 Subduction zone	9.2	30.0	650[d]	1964	5
Kodiak thrust	8.8	30.0	325	1964	5
Kodiak strike-slip	7.5	2.0	325	1845	90

[a] *Schwartz et al.* [2005].
[b] Fault model in which ruptures are allowed to extend from the central to the eastern Denali.
[c] Fault model in which ruptures are allowed to extend from the central Denali to the Totschunda.
[d] *Hamilton and Shennan* [2005].

calculate exceedance probabilities for the National Seismic Hazard Map. First, rupture during the 2002 Denali earthquake branched from the central Denali fault to the Totschunda fault, but new geologic evidence implies that the continuation of rupture onto the eastern Denali fault could be equally likely [*Schwartz et al.*, 2005]. Second, the slip rate on the eastern Denali fault, and to a lesser extent, on the central Denali fault, clearly varies with position along the fault [*Matmon et al.*, 2006].

The first of these issues was addressed by considering two fault models, one including the eastern Denali fault at its full slip rate plus the central Denali fault with 8.4/14.4 of its slip rate, and another model with the Totschunda fault together with the central Denali fault with 6/14.4 of its slip rate. The proportions for the central Denali were derived from the relative partitioning of slip onto the eastern Denali and Totschunda faults. Then, in the hazard codes, earthquakes are allowed to float the full length of the combined faults in each model.

The second modification incorporated into these calculations was the ability to change the frequency of earthquakes of any particular magnitude in proportion to the locally observed slip rate or, equivalently, the annual probability. For example, the characteristic magnitude assumed for the central and eastern Denali fault model was M_w 7.9. In the hazard calculations, the frequency of such earthquakes are assumed to be five times greater along the reach of the fault characterized by a slip rate of 10 mm/yr as contrasted with the reach of the fault characterized by a slip rate of 2 mm/yr. Similarly, when considering earthquakes of lower magnitudes, the same ratio is applied. Although it may be argued that the segments of the faults characterized by higher slip rates might also have a different magnitude distribution (likely with higher magnitudes), we judge the existing modification to be a significant improvement over the previous methodology. This modification was also necessary to account for position-dependent stress changes resulting from regional earthquakes.

3.2. Temporal Models of Recurrence

3.2.1. Poissonian model. Traditional PSHA is time-independent [*Cornell*, 1968; *Frankel et al.*, 2002; *Wesson et al.*, 1999]. The probability of a large earthquake occurring

on a fault segment is independent of whether the last large earthquake happened on the fault yesterday or 500 years ago. Recurrence intervals are observed in the field or derived from slip rates and expected rupture displacements, and the probability of recurrence is equally distributed over all time. There is an expectation, however, that earthquake probabilities should be inherently time-dependent, given that the cause of earthquakes, namely, tectonic stress, is continually driving earthquake recurrence. Simply put, at the beginning of an earthquake cycle, stress on a fault is near a minimum, and hence, an earthquake is least likely. Toward the end, stress approaches a failure threshold, and an earthquake becomes more likely.

3.2.2. Time-dependent models. Although time-dependent probabilities have been described with exponential, gamma, Weibull, and lognormal distributions, we choose the BPT distribution [*Matthews et al.*, 2002] for our analysis. In this model, stress increases linearly from a ground state to a stress threshold. On top of the linear loading, Brownian perturbations are added, which give rise to variability in the recurrence interval. The probability density function (pdf) for this model is given by

$$f(t;\mu,\alpha) = \left(\frac{\mu}{2\pi\alpha^2 t^3}\right)^{1/2} \exp\left\{-\frac{(t-\mu)^2}{2\mu\alpha^2 t}\right\} \quad (1)$$

where f is the probability of having a recurrence time, t, given a mean recurrence, μ, and an aperiodicity, α, which is defined as the standard deviation of the recurrence interval divided by the mean recurrence interval. The hazard rate or the annual probability of rupture given that an earthquake has not occurred since time t is

$$p = \frac{f(t)}{1 - F(t)} \quad (2)$$

where F is the cumulative distribution function of f.

Nishenko and Buland [1987] found that among several candidate distributions, the lognormal distribution best fit their set of normalized recurrence data, although arguments have been made questioning the validity of their method and the small aperiodicity that they derived (0.21) [*Matthews et al.*, 2002; *Savage*, 1991]. We use a relatively standard aperiodicity of 0.5 [*Cramer et al.*, 2000], given that this value for the characteristic faults in this study is relatively uncertain. The BPT model is nearly indistinguishable from the lognormal distribution for up to three recurrence times and has several advantages over the lognormal distribution. The BPT model is based on a physical process and can be considered to reflect the evolution of stress at one point. With increasing time since the last event, the lognormal hazard rate unrealistically tends toward zero probability, whereas the BPT hazard rate tends toward finite probability equal to $(2\mu\alpha^2)^{-1}$. Lastly, steps in stress on target faults and their effect on earthquake probability are easily incorporated in the BPT model. One of the principal problems in applying the BPT model to real faults, however, is that real faults have a significant spatial extent and changes in stress are probably not uniform everywhere on the fault [*Smith*, 2006].

3.2.3. Incorporating stress changes. Coseismic and postseismic stress are calculated from nine regional earthquakes (Plate 2, Table 2; see also *Bufe and Boyd* [this issue]) occurring from 1938 to 2002. The coseismic stresses are calculated for a layered elastic earth model [*Pollitz*, 2005] in the following manner. We use the spherical harmonic solution of *Pollitz* [1996] for the static deformation of a spherically layered model to a point source described with a moment tensor. Finite sources are implemented by integration of a sufficient number of point sources along the rupture plane. This solution, which we refer to as the spectral solution, is truncated at a maximum spherical harmonic degree of 10,000, corresponding to a wavelength of about 4 km. For observation points close to the fault, in order to capture the shorter-wavelength components of the deformation field, the deformation field is realized as the difference of two spectral solutions (that calculated on the layered elastic model, minus that calculated on a homogeneous elastic sphere) added to the homogeneous half-space solution of *Okada* [1992]. This solution is also described by *Banerjee et al.* [2007], and it affords a simple way of capturing a broad spectrum of the elastic deformation field on a layered elastic model. The postseismic stresses are calculated on a vertically layered viscoelastic model [*Pollitz*, 2005] with an elastic upper crust and ductile lower crust and mantle. The mantle has a Burgers body rheology and is characterized by two material relaxation times of 0.05 and 1.3 years based on 19 months of modeled GPS data subsequent to the 2002 Denali earthquake [*Pollitz*, 2005]. Postseismic deformation is calculated by using a viscoelastic normal mode expansion [*Pollitz and Sacks*, 1997], modified for the Burgers body case as described by *Pollitz* [2003].

We apply two methods of incorporating coseismic and postseismic stress changes. The first is a simple consequence of the BPT model. The second is the rate- and state-friction based probability perturbation (RS) introduced by *Hardebeck* [2004]. Alternative methods of incorporating stress changes, which are not used in this analysis, include translating or stretching the probability curve by an amount equal to the stress change divided by the stressing rate. This results

Table 2. Regional Earthquake Source Segments

Latitude, deg	Longitude, deg	Depth, km	Length, km	Width, km	Strike, deg	Dip, deg	Strike-slip, cm	Dip-slip, cm	Year
55.51	–154.46	–5.0	300	150	245.0	10	0	210	1938
53.37	–133.09	0.0	321	12	324.2	90	–800	0	1949
52.43	–131.85	0.0	133	12	311.3	90	–800	0	1949
58.42	–137.12	0.0	227	12	320.0	90	–440	0	1958
57.48	–136.45	0.0	110	12	333.0	90	–440	0	1958
56.98	–150.11	–3.0	100	100	218.0	8	0	550	1964
57.67	–149.08	–3.0	100	100	218.0	8	0	1450	1964
58.38	–148.04	–3.0	100	100	218.0	8	0	70	1964
58.58	–146.62	–2.0	90	100	230.0	8	844	1646	1964
58.95	–145.44	–1.0	90	100	242.0	8	279	1014	1964
59.17	–144.12	–1.0	90	100	256.0	8	18	410	1964
56.99	–152.47	–17.0	100	100	218.0	9	0	410	1964
58.22	–150.28	–17.0	100	100	218.0	9	0	460	1964
58.93	–149.26	–17.0	100	100	218.0	3	349	720	1964
59.32	–147.61	–16.0	120	100	229.0	3	604	2126	1964
59.77	–146.12	–15.0	120	100	241.0	3	113	1786	1964
60.03	–144.40	–15.0	120	100	256.0	3	233	520	1964
60.35	–148.90	–21.0	130	100	219.0	3	20	67	1964
60.57	–146.72	–20.0	130	100	241.0	3	162	2083	1964
60.92	–144.65	–20.0	130	100	256.0	3	61	788	1964
60.05	–147.32	–0.1	72	30	219.0	60	0	850	1964
55.80	–135.29	0.0	190	12	333.0	90	–440	0	1972
59.95	–140.01	–2.0	90	90	271.0	13	0	80	1979
59.25	–142.75	–4.0	112	20	180.0	90	–1070	0	1987
58.19	–142.76	–4.0	125	20	180.0	90	–650	0	1988
62.31	–142.55	0.0	72	12	323.0	90	–225	0	2002
62.87	–143.41	0.0	145	18	296.0	90	–744	0	2002
63.44	–146.05	0.0	55	18	279.0	90	–585	0	2002
63.42	–146.97	0.0	36	18	270.0	48	–150	330	2002

in a clock advance or delay and gives rise to a qualitative appreciation of the effects of stress transfer. The methods used in our paper are more complex; the change to earthquake probabilities depends on when in the earthquake cycle the stress step is applied. A stress step applied later in the earthquake cycle has a greater effect than if applied early in the earthquake cycle.

In the BPT model, Brownian perturbations are superposed onto linear loading. The statistics of this process are realized by allowing the system to elevate to a stress threshold over many earthquake cycles. To develop the statistics for the effects of a stress step, a stress step is applied during each realization at the same time during the earthquake cycle [*Matthews et al.*, 2002]. For this method, we assume an effective coefficient of friction of 0.3 and a characteristic stress drop of 3 MPa.

The second method applies the technique proposed by *Hardebeck* [2004] using rate- and state-dependent fault friction [*Dieterich*, 1994]. This method considers a single stress step, and maps the time-of-failure pdf of a fault to a new pdf reflecting the effects of the stress change. The time-of-failure pdf is thought of as a distribution of hypothetical faults representing the possible states of the real fault. The stress change moves each hypothetical fault toward or away from failure, shifting and deforming the time-of-failure pdf. To implement the method for a stress change history, we

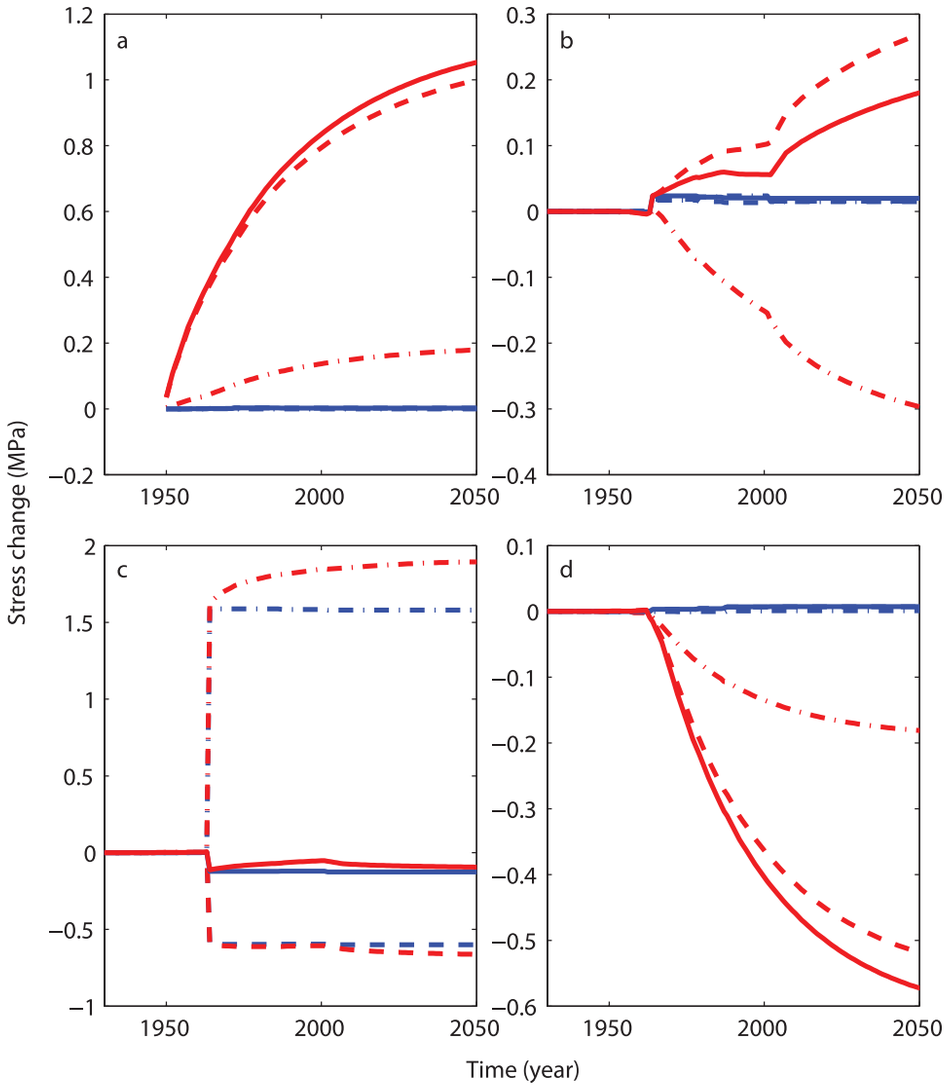

Plate 3. Stress changes at points on the (a) Queen Charlotte, (b) Eastern Denali, (c) Castle Mountain, and (d) Transition faults. Blue curves reflect coseismic stress changes and red curves reflect both coseismic and postseismic stress changes. Solid curves are the Coulomb stress changes, dashed are shear stress changes appropriate for the fault type (a–c, right lateral strike-slip; d, thrust), and dash–dot curves are normal stress changes (positive being tensile).

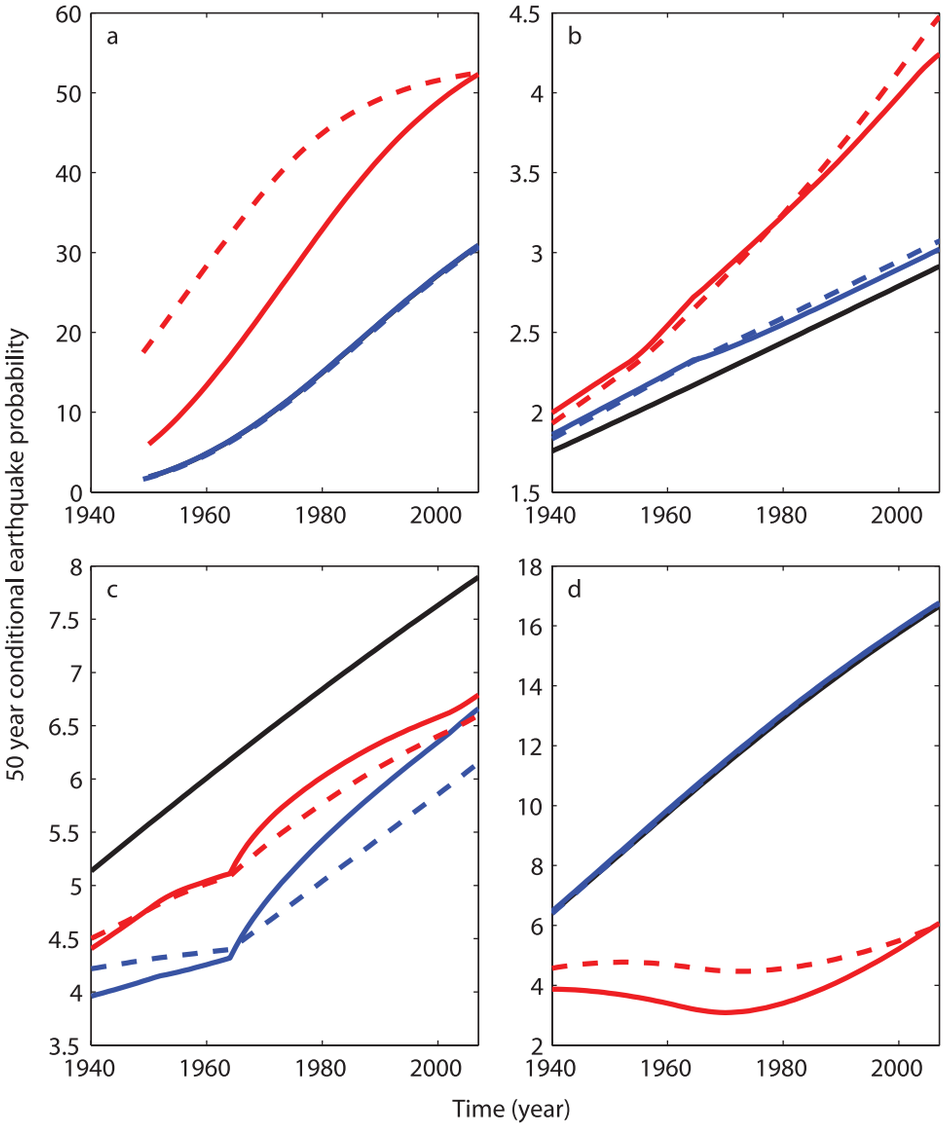

Plate 4. Associated conditional probability curves for the stress changes in Plate 3. Blue curves reflect coseismic stress changes and red curves reflect both coseismic and postseismic stress changes. Solid curves result from BPT stress stepping, whereas dashed curves result from the rate- and state-dependent fault friction stress perturbations to earthquake probabilities. The solid black curve reflects time-dependent probabilities without stress changes.

update the pdf each time step using the incremental stress during that time step. For the first time step, we start with the original BPT time-of-failure pdf determined solely from the recurrence time. For each subsequent time step, we start with the modified pdf found in the last step.

We use *Dieterich's* [1994] formulation of rate- and state-friction as the physical model that determines how the time of failure is changed by a stress step. The new time to failure, T_{new}, for each hypothetical fault is found from the old time to failure, T_{old}, using the relation:

$$T_{new} = \frac{A\sigma}{\tau} \ln\left(\frac{\exp(T_{old}\tau/A\sigma) - 1}{\exp(\Delta CS/A\sigma)} + 1\right) \qquad (3)$$

where the Coulomb stress change $\Delta CS = \Delta\tau + \mu'\Delta\sigma$, with shear stress change $\Delta\tau$, tensional normal stress change $\Delta\sigma$, and effective coefficient of friction $\mu' = 0.3$. The main assumption used to determine the rate and state parameters is that a typical mainshock stress drop is 3 MPa. The parameter $A\sigma$ is set to 0.3 MPa, as *Dieterich* [1994] estimated that $A\sigma$ is ~0.1 of a mainshock stress drop. The stressing rate, τ, is 3 MPa divided by the recurrence time for the receiver fault.

4. STRESS CHANGES

In Plate 3, we present cumulative normal (dashed–dotted), shear (dashed), and Coulomb (solid) stress changes at four locations along the Queen Charlotte, eastern Denali, Castle Mountain, and Transition faults. These locations are indicated as red dots in Plate 1. See *Bufe and Boyd* [this issue] for a more detailed presentation of coseismic Coulomb stress changes due to the earthquakes considered in this study. Normal stresses are defined as tensile such that a positive normal stress change reduces compression across the fault and promotes failure. Coseismic stress changes are blue, whereas coseismic and postseismic stress changes are red. We find that all locations are considerably impacted by the 1964 Prince William Sound earthquake. The Castle Mountain and Eastern Denali are also strongly influenced by the 2002 Denali earthquake. The Queen Charlotte is further influenced by earthquakes along the Queen Charlotte–Fairweather fault system. In all cases but the Castle Mountain, postseismic processes dominate the stress changes.

On the Queen Charlotte fault (Plate 3a), postseismic processes quickly reload the fault subsequent to the 1949 Queen Charlotte earthquake. Postseismic relaxation from the 1964 earthquake act to increase shear and tensile normal stress on the fault, and the combined post-1949 and post-1964 stress changes produce positive Coulomb stress changes. By 2050, the tensile normal stress will have increased by 0.2 MPa and the right-lateral shear stress will have increased by 1 MPa.

The eastern Denali (Plate 3b) fault sees strong and nearly equal postseismic influences from the 1964 Prince William Sound and 2002 Denali earthquakes. Coseismic stress changes are much more apparent for the 1964 earthquake. And although tensile normal stress at this location decreases as a result of these earthquakes, right-lateral shear stress increases by a similar amount leading to a positive Coulomb stress change on the order of 0.2 MPa by 2050.

The Castle Mountain fault (Plate 3c) is of particular interest because of its proximity to Anchorage. This fault is strongly influenced by the 1964 earthquake. Its primary effect has been to increase the tensile normal stress by more than 1.5 MPa. The right-lateral shear stress, however, has decreased and the combined effect, given an effective coefficient of friction of 0.3, is to reduce the Coulomb stress change by about 0.1 MPa.

The Transition fault (Plate 3d) is also of particular interest because of its potential for producing a large tsunamogenic earthquake. Again, the 1964 earthquake has a strong influence on the stress. Tensile normal stress and thrust-sense shear stress are reduced, both conspiring to reduce the Coulomb stress change by almost 0.6 MPa by 2050.

5. EARTHQUAKE PROBABILITIES

Plate 4 shows the associated change in BPT probabilities due to the stress changes in Plate 3. When there are negative (positive) Coulomb stress changes, probability decreases (increases). The amplification of this effect is dependent on the ratio of the Coulomb stress change to the stressing rate or what might be considered the clock change. The shape of this effect, that is, the relative contribution of the modified earthquake probabilities during the earthquake cycle, is dependent on when the clock change is applied. If applied early in the cycle as in the case of the Queen Charlotte fault (Plate 4a), the probability changes are gradual and long-lived. If applied later in the cycle as in the case of the other three localities, the probability change is skewed toward the time of the perturbing event.

For the probabilistic hazard maps, we require annualized rates of earthquake occurrence based on 50-year probabilities beginning in the year 2007. Fifty-year probabilities are obtained by integrating annual rates over 50-year periods. In Plate 5, we present what we consider to be nucleation probabilities within the next 50 years along the characteristic faults of our analysis. *Parsons* [2005] recommends drawing stress change values from a distribution that reflects the spatial pattern of stress change rather than using the mean, which may overstate earthquake probabilities. Since we float

ruptures along our faults, which are generally longer than the characteristic rupture lengths, we do not think that a single value of stress change is appropriate. Hence, to obtain earthquake probabilities from nucleation probabilities, we smooth the latter with a Gaussian function having a dominant wavelength equal to the characteristic rupture length (Table 1), which is derived from the analysis of *Wells and Coppersmith* [1994]. In Plate 6, we show, for all of our characteristic faults, how the time-dependent earthquake probabilities have changed relative to time-independent ones. Roughness, particularly in the postseismic results, is due to variability in fault strike and resolving shear and normal stresses onto that plane, as well as proximity to the sources.

For most faults, postseismic processes dominate changes in earthquake probabilities. The BPT model appears to be insensitive to postseismic stress changes soon after the event, whereas the RS model is very sensitive; the central Denali, where the greatest slip occurred during the 2002 earthquake, is quickly reloaded by viscoelastic relaxation in the lower crust and upper mantle, increasing 50-year earthquake probabilities in the RS model to more than twice the time-independent rate. The same phenomenon for the RS model relative to the BPT is apparent for the subduction zone in the region of the 1964 earthquake.

6. RESULTING EARTHQUAKE HAZARD

To derive the earthquake hazard, we couple the rates of earthquake occurrence outlined above with the ground-motion relations described by *Wesson et al.* [2007]. Unfortunately, ground-motion prediction equations specific to Alaska have not been developed. Therefore, equations developed for the Western United States and other regions have been used.

In general, earthquake hazard is directly proportional to earthquake probabilities. But since there is a time-independent background seismicity component, and characteristic fault behavior (time-dependent) is weighted equally with Gutenberg–Richter fault behavior (time-independent), changes in seismic hazard are not as great as might be expected. Furthermore, smaller, more frequent earthquakes in the Gutenberg–Richter component of a seismic hazard model tend to contribute more to seismic hazard than an equal contribution (with respect to moment released) from a characteristic component. *Wesson et al*. [this issue] present the component hazard curves for Anchorage, which sits above the Prince William Sound segment of the subduction zone and near the Castle Mountain fault, where we find that, perhaps counterintuitively, background seismicity has the largest contribution. If we give full weight to characteristic behavior rather than weighing it equally with Gutenberg–Richter, we find that this modification changes seismic hazard at Anchorage by less than 1%.

The Gutenberg–Richter component still plays a primary role very close to the fault source. Along much of the central Denali fault where the 2002 earthquake occurred, peak ground accelerations with a 2% probability of exceedance in 50 years are down about 10%, yet earthquake probabilities for characteristic fault behavior are down nearly 100%. At 1 s spectral acceleration, changes to probabilistic ground motions are amplified by about a factor of 2. This larger difference in hazard results from the fact that ground motion prediction equations suggest that larger earthquakes will have a greater contribution to seismic ground motions at longer periods relative to smaller earthquakes.

Some areas of Alaska do not have a time-independent component that is weighted equally with the time-dependent characteristic component. According to *Wesson et al*. [2007], such areas have faults that are considered "A-type" or those that are considered to be well characterized and follow characteristic behavior for magnitudes greater than 8. These include the Transition fault, and the Prince William Sound region of the subduction zone. However, these regions still have a substantial background component, which tends to dilute the characteristic contribution to seismic hazard.

Even though hazard adjacent to a characteristic fault source may change by 10%, hazard at most cities is unchanged (Table 3). For example, of the 24 cities listed in Table 3, only Kodiak, Paxson, Sitka, Delta Junction, and Tok have substantially modified hazard. Of those, Sitka is unaffected by stress transfer. The others are more sensitive to the RS model with coseismic and postseismic stress changes, generally raising seismic hazard above the time-independent level.

7. DISCUSSION

Performing a time-dependent analysis can be fairly straightforward, but the uncertainty associated with the assumptions and parameters necessary for the analysis can be significant. Are the fault sources truly characteristic? Do they rupture with a single magnitude and have complete stress drop [*Wesson and Boyd*, 2007]? How well known is the variation in recurrence interval? Our analysis is preliminary, and we do not attempt to solve many of the issues discussed below.

7.1. Characteristic Magnitude

For characteristic faults that ruptured within the last 100 years, magnitudes can be assigned [see *Bufe and Boyd*, this issue]. Otherwise, magnitudes are derived from the fault

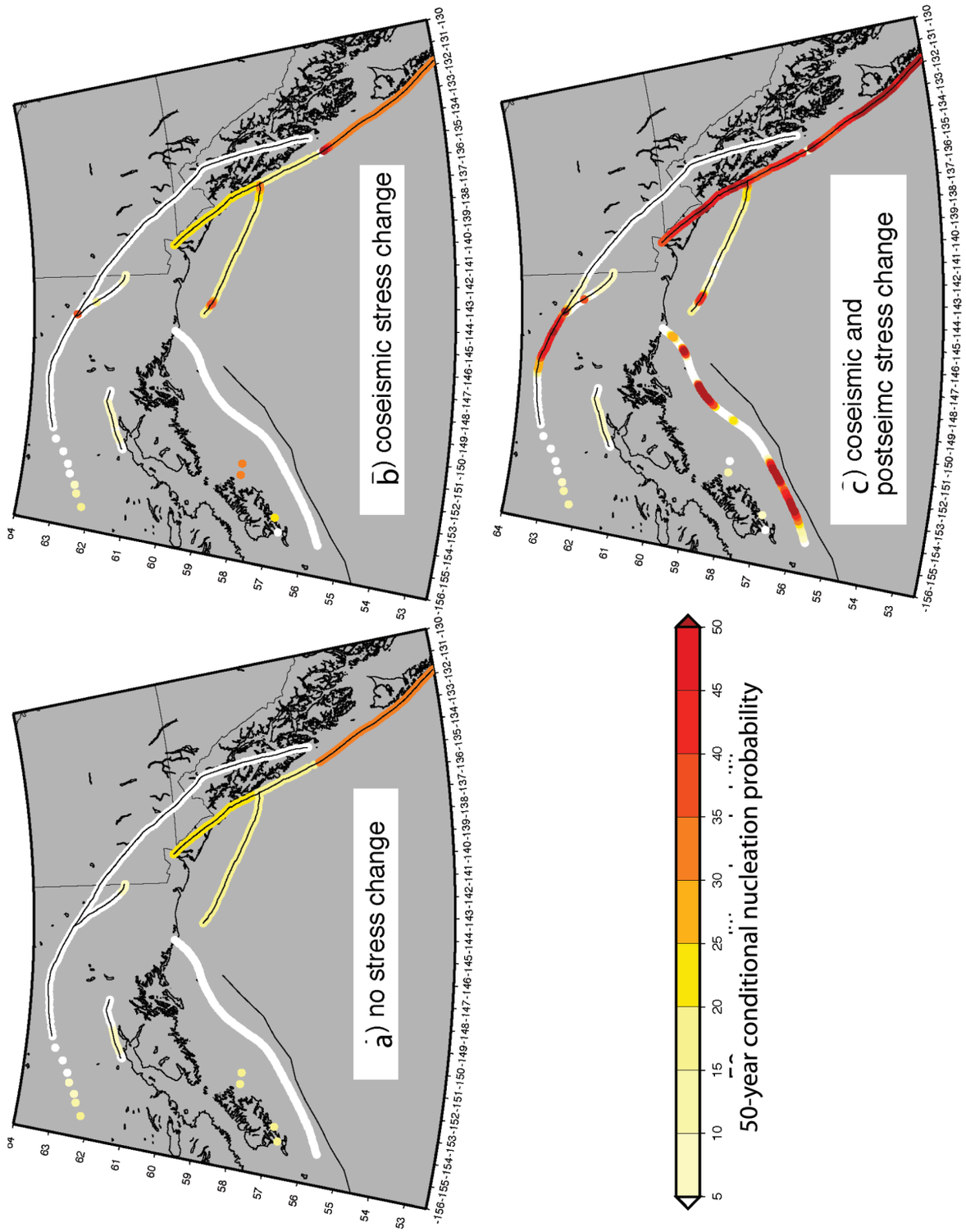

Plate 5. Time-dependent 50-year nucleation probabilities (a) without stress changes, (b) with coseismic rate- and state-dependent stress changes, and (c) with coseismic and postseismic rate- and state-dependent stress changes for the target faults in this study.

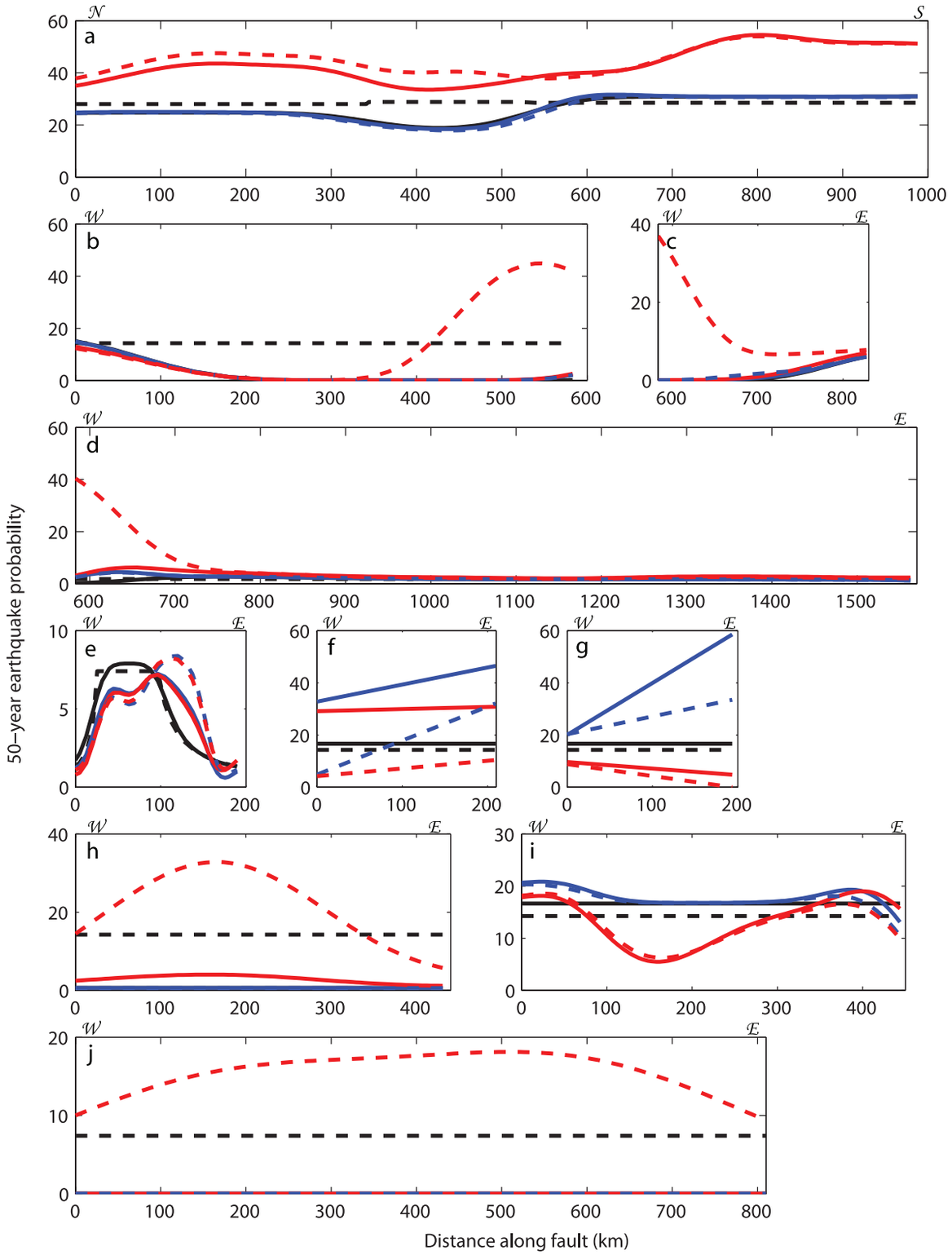
a
b
c
d
e
f
g
h
i
j
N
S
W
E
50–year earthquake probability
Distance along fault (km)

Table 3. Fifty-Year Probabilistic Ground Motions for Selected Cities in Alaska

			2% Probability of Exceedance in 50 years, %											
			PGA						1 s SA					
				BTP			RS			BPT			RS	
City	Lat.	Long.	TI[a]	NS[b]	C[c]	CP[d]	C	CP	TI	NS	C	CP	C	CP
Anchorage	61.17	–150.02	69	69	69	69	69	69	62	62	62	62	62	62
Wasilla	61.62	–149.37	78	78	78	78	79	79	74	73	74	74	76	76
Fairbanks	64.82	–147.87	41	41	41	41	41	41	30	30	30	30	30	31
Juneau	58.37	–134.58	25	27	27	27	27	27	29	30	30	30	30	30
Ketchikan	55.35	–131.70	11	18	18	18	18	18	19	20	20	20	20	20
Kodiak	57.75	–152.50	71	71	72	72	70	70	76	76	78	78	75	75
Bethel	60.78	–161.80	13	12	12	12	12	12	10	10	10	10	10	10
Nome	64.50	–165.43	23	23	23	23	23	23	16	16	16	16	16	16
Kotzebue	66.87	–162.63	17	17	17	17	17	17	13	13	13	13	13	13
Barrow	71.30	–156.87	1	1	1	1	1	1	0	0	0	0	0	0
Prudhoe Bay	70.25	–148.33	13	13	13	13	13	13	9	9	9	9	9	9
McGrath	62.97	–155.62	17	17	17	17	17	17	16	15	15	15	15	15
Dillingham	59.05	–158.52	12	12	12	12	12	12	14	14	14	14	14	14
Valdez	61.13	–146.35	64	64	64	64	64	64	66	66	66	66	66	66
Homer	59.63	–151.50	64	64	64	64	64	64	58	58	58	58	58	58
Kenai	60.57	–151.25	62	62	62	62	62	62	51	51	51	51	51	51
Paxson	63.03	–145.50	33	30	31	31	31	39	41	35	35	36	35	53
Yukatat	59.52	–139.67	65	65	65	65	65	65	70	72	72	72	72	72
Haines Harbor	59.23	–139.43	71	71	71	71	71	71	82	81	81	81	81	81
Sitka	57.07	–135.35	32	48	48	48	48	48	46	80	80	80	80	80
Dutch Harbor	53.88	–166.53	64	64	64	64	64	64	54	54	54	54	54	54
Delta Junction	64.00	–145.50	27	26	26	26	26	27	27	25	25	25	25	33
Tok	63.30	–143.00	20	18	18	19	18	22	26	23	24	24	24	32
Glenmallen	62.00	–146.60	47	47	47	47	47	47	44	44	44	44	44	44

[a] Time-independent.
[b] No stress.
[c] Coseismic.
[d] Coseismic and postseismic.

length or slip rate and characteristic recurrence interval using the *Wells and Coppersmith* [1994] relations. For fault models consisting of several fault segments, which would otherwise have a characteristic magnitude for each segment, a single magnitude is considered. This decision results from current limitations in the hazard codes. We do not consider strict segmentation but allow our ruptures to float along the entire length of the fault.

7.2. Recurrence Interval and Variability

Recurrence intervals are obtained geologically for only a subset of the characteristic faults. For all other characteristic faults, it is calculated by using the slip rate, magnitude, and fault dimensions. The very few observed recurrence intervals leads to large uncertainties in both the mean and standard deviation of the recurrence interval. Where calculations

Plate 6. (Opposite) Fifty-year conditional earthquake probabilities beginning in 2007 for the nine target faults in this study: (a) Queen Charlotte–Fairweather fault system, (b) Central Denali, (c) Totschunda and Cross Creek, (d) Eastern Denali, (e) Castle Mountain, (f) Kodiak Island, (g) Narrow Cape, (h) Kodiak segment of the subduction zone, (i) Transition, (j) 1964 area of the subduction zone. Dashed black curves are time-independent estimates. Solid black curves are time-dependent estimates without stress changes. Blue curves reflect estimates based on coseismic stress changes and red curves reflect both coseismic and postseismic stress changes. Solid red and blue curves result from BPT stress stepping, whereas dashed red and blue curves result from the rate- and state-dependent fault friction stress perturbations to earthquake probabilities.

cannot be easily made, we assume that the faults are strongly influenced by large subduction zone earthquakes and assign the same recurrence interval. Consistent with other studies [*Cramer et al.*, 2000; *WGCEP94*, 1995], we choose an aperiodicity, which is a measure of the recurrence interval variability, of 0.5.

7.3. Time of the Last Earthquake

Precise dates exist for earthquakes that have ruptured within the last century. Geological observations have identified the most recent events on a limited number of faults such as the Denali [*Schwartz et al.*, 2005] and Prince William Sound segment of the subduction zone [*Hamilton and Shennan*, 2005]. We have assumed that where this value is unknown, the fault is halfway through its recurrence interval, thereby resulting in a time-dependent probability that is similar to the time-independent value.

7.4. Stress on Faults

The stress change on target faults due to regional earthquakes suffers from considerable uncertainty resulting from not knowing specific details about earthquake ruptures or intervening rheological parameters. Slip models for many past earthquakes are heavily simplified, generally described by a single rupture plane having uniform slip. The slip models do not incorporate afterslip on either the source or target faults. For target fault segments located more than a fault width from the perturbing event, the finer details of the slip model become negligible (Saint-Venant's principle; *Timoshenko and Goodier* [1951]). But for target faults adjacent to the perturbing event, this information becomes very important.

Between the perturbing event and the target fault, the rheological parameters of the intervening material play a critical role. The rheological model that we use is one-dimensional, although we know that there is significant three-dimensional spatial variability owing primarily to the subduction zone. Furthermore, effects due to poroelasticity have not been accounted for in our stress modeling.

7.5. Time-Dependent Probability Model

The time-dependent probability models that we consider contain the assumptions that the stress threshold at which an earthquake nucleates (or, for the rate-and-state model, the critical slip rate) and the stress drop are constant, and that the loading is linear. Observations suggest that although earthquake recurrence on characteristic fault segments may be lognormally distributed [*Nishenko and Buland*, 1987; *Weldon et al.*, 2004], the stress threshold and/or stress drop may not be constant [*Weldon et al.*, 2004]. Additionally, the loading may not be linear, as modeled by *Michael* [2005].

The modeling of *Michael* [2005] highlights a subtle drawback of our methodology. In addition to perturbing the stress and earthquake probability on other faults, the postseismic relaxation can reload or unload parts of the fault segment that ruptured in the event, depending on the specifics of the slip distribution and the orientation of the segment. If the fault is reloaded by postseismic processes, this will cause the fault segment to be closer to failure for a greater amount of time during the seismic cycle relative to linear tectonic loading. For a given amount of randomness in the loading process, postseismic reloading increases the coefficient of variation, as shown by *Michael* [2005]. If the coefficient of variation in our underlying time-dependent BPT distribution already accounts for postseismic reloading (or unloading as the case may be), we would, in essence, be double-counting these postseismic effects. In the case of postseismic reloading, it would then be more accurate to start with a lower coefficient of variation, such that the variation obtained after including the postseismic reloading matched the observed variability. One effect of an inappropriately high variability is to increase the probability at short repeat times, which in part explains the relatively high event probabilities along some of the fault segments that have produced historic earthquakes. This is a problem of current and future research and will be addressed in subsequent work.

8. CONCLUSIONS

Calculated earthquake probabilities can be significantly affected by time-dependent processes. Because of the recent large earthquakes on the Denali fault and Prince William Sound segment of the subduction zone (relative to their recurrence intervals), characteristic ruptures on these faults now have a low probability of rupture. In contrast, earthquake probabilities on neighboring faults, such as the Castle Mountain, Cross Creek, or eastern Denali faults, which may be advanced in their earthquake cycles, can be strongly influenced by regional stress changes.

Segments neighboring the central Denali are strongly affected by the 2002 earthquake. Coseismic stress changes strongly impacted earthquake probabilities on the eastern Denali, western Denali, and Cross Creek faults. As we are further removed from the time of the 2002 earthquake, postseismic relaxation will diffuse stress over a greater extent, further modifying probabilities for characteristic rupture on these segments.

The Fairweather–Queen Charlotte fault system is strongly influenced by postseismic relaxation, characteristic earth-

quake probabilities having been increased by up to 100% along much of its length. The Transition fault too has been considerably affected by postseismic relaxation, reducing the probability of rupture near its center to close to zero.

Seismic hazard may change adjacent to characteristic faults by 10% or more. However, because of our method of combining time dependence with time independence, time-dependent seismic hazard at most cities in Alaska is virtually unchanged. Additional work is needed to address the time-dependent component of the background seismicity. Research is also needed to address how much seismic moment should be partitioned between a single characteristic magnitude and a logarithmic Gutenberg–Richter distribution of magnitudes or whether a more sophisticated distribution is needed. Furthermore, large uncertainties exist in key parameters such as characteristic magnitude, mean recurrence interval and its variability, and the time of the last earthquake. These quantities must be addressed with additional research to make time-dependent probabilistic seismic hazard maps more meaningful and applicable.

Acknowledgments. This work benefited substantially from the reviews of Ruth Harris, David Perkins, and Goran Ekstrom. Funding was provided by the National Seismic Hazard Mapping project of the U.S. Geological Survey.

REFERENCES

Banerjee, P., et al. (2007), Coseismic slip distributions of the 26 December 2004 Sumatra–Andaman and 28 March 2005 Nias earthquakes from GPS static offsets, *Bull. Seismol. Soc. Am.*, *97*(1A), S86–S102.

Bufe, C. G., and O. S. Boyd, Fault interaction in Alaska: Coulomb stress transfer, in *Active Tectonics and Seismic Potential of Alaska*, *AGU Monogr*., edited by J. Freymueller, et al., this volume.

Cornell, A. (1968), Engineering seismic risk analysis, *Bull. Seismol. Soc. Am.*, *58*(5), 1583–1606.

Cramer, C. H., et al. (2000), A time-dependent probabilistic seismic-hazard model for California, *Bull. Seismol. Soc. Am.*, *90*(1), 1–21.

DeMets, C., and T. H. Dixon (1999), New kinematic models for Pacific–North America motion from 3 Ma to present: I. Evidence for steady motion and biases in the NUVEL-1A model, *Geophys. Res. Lett.*, *26*(13), 1921–1924.

Dieterich, J. (1994), A constitutive law for rate of earthquake production and its application to earthquake clustering, *J. Geophys. Res.*, *99*, 2601–2618.

Eberhart-Phillips, D., et al. (2003), The 2002 Denali fault earthquake, Alaska: A large magnitude, slip-partitioned event, *Science*, *300*(5622), 1113–1118.

Engdahl, E. R., and A. Villaseñor (2002), Global seismicity: 1900–1999, in *International Handbook of Earthquake and Engineering Seismology*, edited by W. H. K. Lee, et al., pp. 665–690, IASPEI.

Frankel, A. D., et al. (2002), Documentation for the 2002 update of the National Seismic Hazard Maps, *U.S. Geol. Surv. Open-File Rep.*, *2002-420*.

Freed, A. M., and J. Lin (2001), Delayed triggering of the 1999 Hector Mine earthquake by viscoelastic stress transfer, *Nature*, *411*, 180–183.

Freed, A. M., et al. (2006), Implications of deformation following the 2002 Denali, Alaska, earthquake for postseismic relaxation processes and lithospheric rheology, *J. Geophys. Res.*, *111*, B01401, doi:10.1029/2005JB003894.

Gardner, J. K., and L. Knopoff (1974), Is the sequence of earthquakes in southern California, with aftershocks removed, Poissonian?, *Bull. Seismol. Soc. Am.*, *64*(5), 1363–1367.

Haeussler, P. J., et al. (2004a), Surface rupture of the 2002 Denali Fault, Alaska, earthquake and comparison with other strike-slip ruptures, *Earthq. Spectr.*, *20*(3), 565–578.

Haeussler, P. J., et al. (2004b), Surface rupture and slip distribution of the Denali and Totschunda Faults in the 3 November 2002 *M* 7.9 earthquake, Alaska, *Bull. Seismol. Soc. Am.*, *94*(6B), S23–S52.

Hamilton, S., and I. Shennan (2005), Late Holocene relative sea-level changes and the earthquake deformation cycle around upper Cook Inlet, Alaska, *Quat. Sci. Rev.*, *24*, 1479.

Hardebeck, J. L. (2004), Stress triggering and earthquake probability estimates, *J. Geophys. Res.*, *109*, B04310, doi:10.1029/2003JB002437.

Harris, R. A., and R. W. Simpson (1992), Changes in static stress on southern California faults after the 1992 Landers earthquake, *Nature*, *360*(6401), 251–254.

Harris, R. A., and R. W. Simpson (1996), In the shadow of 1857 — the effect of the great Fort Tejon earthquake on subsequent earthquakes in southern California, *Geophys. Res. Lett.*, *23*, 229–232.

Jaumé, S. C., and L. R. Sykes (1996), Evolution of modern seismicity in the San Francisco Bay region, 1850 to 1993: Seismicity changes related to the occurrence of large and great earthquakes, *J. Geophys. Res.*, *101*, 765–789.

Johnson, J. M., et al. (1996), The 1964 Prince William Sound earthquake: Joint inversion of tsunami and geodetic data, *J. Geophys. Res.*, *101*, 523–532.

Kenner, S. J. (2004), Rheological controls on fault loading rates in northern California following the 1906 San Francisco earthquake, *Geophys. Res. Lett.*, *31*, L01606, doi:10.1029/2003GL018903.

King, G. C. P., et al. (1994), Static stress changes and the triggering of earthquakes, *Bull. Seismol. Soc. Am.*, *84*, 935–953.

Matmon, A., et al. (2006), Denali Fault slip rates and Holocene–late Pleistocene kinematics of Central Alaska, *Geology*, *34*(8), 645–648.

Matthews, M. V., et al. (2002), A Brownian model for recurrent earthquakes, *Bull. Seismol. Soc. Am.*, *92*(6), 2233–2250.

Michael, A. J. (2005), Viscoelasticity, postseismic slip, fault interactions, and the recurrence of large earthquakes, *Bull. Seismol. Soc. Am.*, *95*(5), 1594–1603.

Nishenko, S., and R. Buland (1987), A generic recurrence interval for earthquake forecasting, *Bull. Seismol. Soc. Am.*, *77*, 1382–1389.

Okada, Y. (1992), Internal deformation due to shear and tensile faults in a half space, *Bull. Seismol. Soc. Am.*, *82*, 1018–1040.

Parsons, T. (2005), Significance of stress transfer in time-dependent earthquake probability calculations, *J. Geophys. Res.*, *110*, B05S02, doi:10.1029/2004JB003190.

Parsons, T., et al. (2000), Heightened odds of large earthquakes near Istanbul: An interaction-based probability calculation, *Science*, *288*, 661–664.

Pollitz, F. F. (1996), Coseismic deformation from earthquake faulting on a layered spherical Earth, *Geophys. J. Int.*, *125*, 1–14.

Pollitz, F. F. (2003), Transient rheology of the uppermost mantle beneath the Mojave Desert, California, *Earth Planet. Sci. Lett.*, *215*, 89–104.

Pollitz, F. F. (2005), Transient rheology of the upper mantle beneath central Alaska inferred from the crustal velocity field following the 2002 Denali earthquake, *J. Geophys. Res.*, *110*, B08407, doi:10.1029/2005JB003672.

Pollitz, F. F., and I. S. Sacks (1997), The 1995 Kobe, Japan, earthquake: A long-delayed aftershock of the offshore 1944 Tonankai and 1946 Nankaido earthquakes, *Bull. Seismol. Soc. Am.*, *87*, 1–10.

Pollitz, F. F., and I. S. Sacks (2002), Stress triggering of the 1999 Hector Mine earthquake by transient deformation following the 1992 Landers earthquake, *Bull. Seismol. Soc. Am.*, *92*, 1487–1496.

Pollitz, F. F., et al. (2001), Mantle flow beneath a continental strike-slip fault: Postseismic deformation after the 1999 Hector Mine earthquake, *Science*, *293*, 1814–1818.

Reasenberg, P. A., and R. W. Simpson (1992), Response of regional seismicity to the static stress change produced by the Loma–Prieta earthquake, *Science*, *255*(5052), 1687–1690.

Savage, J. C. (1991), Criticism of some forecasts of the National Earthquake Prediction Evaluation Council, *Bull. Seismol. Soc. Am.*, *81*, 862–881.

Schwartz, D. P., and K. J. Coppersmith (1984), Fault behavior and characteristic earthquakes: Examples from the Wasatch and San Andreas fault zones, *J. Geophys. Res.*, *89*(B7), 5681–5698.

Schwartz, D. P., et al. (2005), Unraveling the earthquake history of the Denali fault system, Alaska—Filling a blank canvas with paleoearthquakes, *Eos Trans. AGU, Fall Meet. Suppl.*, *86*(52), Abstract U42A–06.

Smith, D. E. (2006), A new paradigm for interpreting stress inversions from focal mechanisms: How 3D stress heterogeneity biases the inversions toward the stress rate, Ph.D. dissertation, California Institute of Technology, Pasadena.

Stein, R. S. (1999), The role of stress transfer in earthquake occurrence, *Nature*, *402*, 605–609.

Stein, R. S., et al. (1997), Progressive failure on the North Anatolian fault since 1939 by earthquake stress triggering, *Geophys. J. Int.*, *128*, 594–604.

Stover, C. W., and J. L. Coffman (1993), Seismicity of the United States, 1568–1989 (revised), *U.S. Geol. Surv. Prof. Pap.*, *1527*, 418 pp.

Thenhaus, P. C., et al. (1985), Probabilistic estimates of maximum seismic horizontal ground acceleration on rock in Alaska and the adjacent continental shelf, *Earthq. Spectr.*, *1*, 285–306.

Timoshenko, S., and J. N. Goodier (1951), Saint-Venant's principle, in *Theory of Elasticity*, McGraw-Hill, New York.

Toda, S., et al. (1998), Stress transferred by the 1995 M_w = 6.9 Kobe, Japan, shock: Effect on aftershocks and future earthquake probabilities, *J. Geophys. Res.*, *103*, 24,543–24,565.

Weldon, R., et al. (2004), Wrightwood and the earthquake cycle: What a long recurrence interval tells us about how faults work, *GSA Today*, *14*(9), 4–10.

Wells, D. L., and K. J. Coppersmith (1994), New empirical relationships among magnitude, rupture length, rupture width, rupture area, and surface displacement, *Bull. Seismol. Soc. Am.*, *84*(4), 974–1002.

Wesson, R. L., and O. S. Boyd (2007), Stress before and after the 2002 Denali fault earthquake, *Geophys. Res. Lett.*, *34*, L07303, doi:10.1029/2007GL029189.

Wesson, R. L., et al. (1999), Probabilistic Seismic Hazard Maps of Alaska, *U.S. Geol. Surv. Open File Rep.*, *99-36*.

Wesson, R. L., et al. (2007), Revision of time-independent probabilistic seismic hazard maps for Alaska, *U.S. Geol. Surv. Open File Rep.*, *2007-1043*.

Wesson, R. L., et al., Issues in making a seismic hazard map for Alaska and the Aleutians, in *Active Tectonics and Seismic Potential of Alaska*, *AGU Monog*r., edited by J. Freymueller, et al., this volume.

WGCEP94 (1995), Seismic hazards in southern California: Probable earthquakes, 1994–2024, *Bull. Seismol. Soc. Am.*, *85*, 379–439.

O. S. Boyd, C. G. Bufe, R. L. Wesson, and Y. Zeng, U.S. Geological Survey, Golden, CO 80401, USA. (olboyd@usgs.gov)

J. L. Hardebeck and Fred Pollitz, U.S. Geological Survey, 345 Middlefield Road MS 977, Menlo Park, CA 94025, USA.